Modeling of Lanthanide Transport in Metallic Fuels: Recent Progresses

C.Unal[1], L. Xiang[2], J.Isler[2], C.Matthews[1], S.Abid[2], J.Zhang[2], J.Galloway[1], R.Mariani[3]

[1]Los Alamos National Laboratory, Los Alamos, NM, USA

[2]Ohio State University, Columbus, Ohio, US

[3]Idaho National Laboratory, Idaho Falls, ID, USA

E-mail contact of main author: cu@lanl.gov

Abstract. Experimental and modeling efforts are underway to determine the solubility and diffusivity of certain lanthanides in liquid metals to assess the feasibility of a liquid-like lanthanide transport (1) mechanism in metallic fuels. Using ab-initio Molecular Dynamics (AIMD), the solubility of cerium in liquid sodium at 1000 K was calculated to be less than 0.8 at.%. The diffusion coefficient of cerium in liquid sodium was calculated to be 5.6 10^{-5} cm^2/s [2]. We extended the MD work to include two temperatures, 723 K and 1000 K, for the diffusion of cerium (Ce), praseodymium (Pr), and neodymium (Nd) in both sodium (Na) and cesium (Cs) [3]. The lanthanide diffusivities were found to be in the same order of magnitude observed in liquid diffusion (10^{-5} cm^2/s) and the temperature dependence of the diffusivity was developed according to the Arrhenius equation. Experiments have been performed to measure the solubility of lanthanides in liquid sodium. While using ICP-MS is used to measure the concentration of a particular lanthanide in a sodium sample, the solubility at that testing temperature is calculated. The experimental results indicated that the solubility of cerium, praseodymium, and neodymium in liquid sodium varied from 1×10^{-5} to 3×10^{-5} at.% in the temperature range of 723 to 823 K. The time dependence of dissolution was also obtained from experiments conducted at different equilibration times. The results showed that the solubility limit was reached within 30 minutes, indicating the dissolution rate is likely high relative to diffusion, thus suggesting lanthanide transport in liquid metals would be diffusion limited. We developed a conceptual pore model to better describe the lanthanide transport behavior through the fuel. Our results suggests that isolated pores will most likely act as a lanthanide sink and that the transport mechanism of lanthanides from fuel to cladding must occur through interconnected pores and cracks which are filled with sodium.

Key Words: Lanthanide, Solubility, Diffusivity, Transport

1. Introduction

Understanding the nature of lanthanide transport in metallic fuels and its relation to fuel/cladding chemical interaction (FCCI) has long been a topic of interest yet short on data. A "liquid-like" transport mechanism for lanthanide (Ln) fission products was recently proposed based on post irradiation experimental (PIE) data obtained from Experimental Breeder Reactor-II (EBR-II) [1]. This model is based on the conjecture that fission products may transport as solutes in liquid metals, such as liquid cesium or a cesium-sodium mixture. The proposed mechanism can qualitatively account for the Ln migration to the fuel peripheral surface and the deposition observed as a sludge-like form on the inner radius of the cladding. To better describe the Ln transport behavior and examine the liquid-like mechanism, the acquisition of fundamental data such as Ln diffusion coefficients in liquid sodium is necessary. Moreover the knowledge of diffusivity in liquid metals is important for prediction of mass transfer rates which plays an important role in several applications such as corrosion, phase separation, and crystal growth. The U.S. Department of Energy recently supported a project to study the lanthanide transport process both experimentally and analytically under its

Nuclear Energy University Program. This paper summarizes the progress made during last two and half years. We first discuss AIMD studies to obtain the solubility and diffusivity of lanthanides in sodium and cesium. Next, we discuss experimental results on solubility measurements. Calculated properties along with the experimental data are used in a 1-D model to check the feasibility of liquid-like transport mechanism. We briefuly discuss this model and summarize initial conclusions.

2. Solubility and Diffusivity of Lanthanides by Ab-Initio Molecular Dynamic Simulations

Samin et al. [2] employed AIMD simulations to explore the solubility and diffusivity of cerium in liquid sodium at elevated temperatures. FIG. 1 shows the change in chemical potential ($\Delta\mu_l$) of cerium in liquid sodium. The data was collected by performing insertions of single atoms into a system of sodium atoms, that is one Ce in 256 Na, one Ce in 128 Na, and one Ce in 124 Na/4Ce atoms, and comparing the excess chemical potential with a baseline of one Ce in 32 Ce. This change is initially negative but becomes positive at about 0.4–0.6 at.%. The DFT solubility limit appears to be between 0.4 and 0.6 at% at a temperature of 1000 K. However, when the uncertainty in the calculation is accounted for, we can only conclude with confidence that the solubility limit is lower than 0.78 at.% at 1000 K. Our reported solubility was consistent with the known experimental results for similar materials at high temperatures (see [2]). In the next section we will compare the calculated solubility with our current data. .

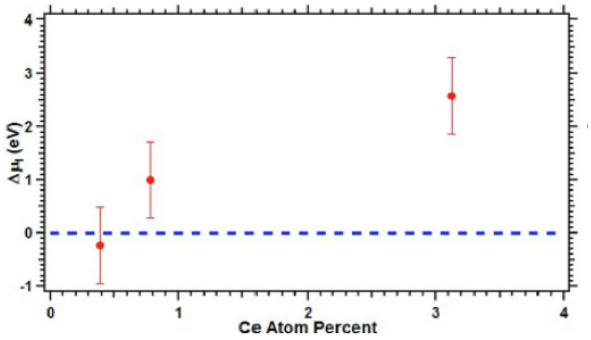

FIG. 1. Change in chemical potential of cerium upon solvation in a cerium/sodium melt, given as a function of the molar concentration of cerium in the liquid sodium at 1000 K

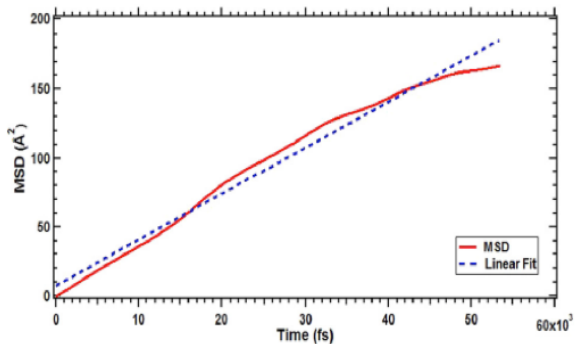

FIG. 2. This plot was recorded for four Ce atoms diffusing in 124 Na atoms at 1000 K. The mean square displacement of the four-cerium atoms is plotted against time.

The diffusivity of cerium in liquid sodium at 1000 K was calculated by recording the mean-square displacement for four cerium atoms in a system of 124 sodium atoms. The data was recorded after allowing the system to equilibrate for 5 ps in the canonical ensemble using the Nose-Hoover thermostat for 160 ps. The data was then analyzed to report the mean square displacement over 50 ps. FIG. 2 shows the calculated mean squared displacement (MSD) values which were collected over 50 ps after allowing the simulation to equilibrate for 5 ps. After fitting a linear plot to the data and examining the slope, one can calculate the diffusion coefficient at 1000 K. The best linear fit (a+bx) yields a=7.4±0.27 and b=0.0033±8.85 $\times 10^{-6}$. This in turn yields a diffusivity of 5.6×10^{-5} cm^2/s. Again, the experimental value for this quantity is currently unknown; however, this value seems reasonable when compared with other experimental data for the diffusion of cerium in other similar materials at elevated temperatures.

Subsequently we extended AIMD simulations to higher temperatures (523 K, 723 K, 923 K, 1000 K) [3] and investigated three abundant Ln fission product diffusion coefficients in liquid Na at multiple temperatures. The diffusivity of Ln in liquid metals can be calculated from the Ln mean-square displacement (MSD) based on the Einstein-Stokes equation. The diffusion coefficient for Ce in liquid Na at 723 K was calculated by recording the mean square displacements of four Ce atoms in the liquid metallic system of 124 Na atoms for more than 50 ps. The slope of the fitting data can be used to obtain the diffusivities for three Ln atoms at different temperatures, as listed in Table 1. The diffusion coefficients of Ln in liquid Na were all found to be on the order of 10^{-5} cm^2/s. Additionally the diffusivity for each metallic system increased with temperature as expected, while the corresponding experimental values are still lacking. However, other experimental data for the diffusion of specific Ln in other similar systems at elevated temperatures can provide some support. For example, our simulation data show reasonable agreement with previous experimental studies on the diffusion of cerium oxy ions in a $MgCl_2$-NaCl-KCl eutectic at 853 K, which yields a diffusion coefficient on the order of 10^{-5} cm^2/s [3]. Moreover, the diffusivity of K in a system of $Na_{90}Li_{10}$ at 373 K is calculated to be 4.77×10^{-5} cm^2/s in a classical molecular study of the Na-K alloy [3].

TABLE I: LN DIFFUSIVITY IN LIQUID NA [3].

System	**Temperature (K)**	**Diffusivity ($10^5\times cm^2/s$)**
Ce in Na	523	1.04 ± 0.07
	723	1.94 ± 0.14
	1000	5.34 ± 0.13
Pr in Na	723	4.53 ± 0.29
	923	6.01 ± 0.34
Nd in Na	723	4.00 ± 0.27
	923	4.63 ± 0.28

TABLE 2: NA DIFFUSIVITY IN VARIOUS METALLIC SYSTEMS [3].

System	**Temperature (K)**	**Diffusivity ($10^5 \times cm^2/s$)**
Na	723	12.76 ± 0.51
	923	17.76 ± 0.83
Na (EAM) [5]	573	11.5
	723	16.4
Na (Experimental) [6]	573	13
Ce in Na	723	12.30 ± 0.62
	1000	22.92 ± 0.72
Pr in Na	723	8.07 ± 0.21
	923	13.73 ± 0.48
Nd in Na	723	8.25 ± 0.29
	923	12.77 ± 0.58

Table 1 shows that the diffusion coefficient of Ce has the strongest dependence on temperature. One possible reason is that Na-Ce is in the intermediate state between solid and liquid as discussed above and an increase in temperature facilitates transition of the metallic system to the liquid state with a larger diffusion coefficient. Furthermore, no conclusions may be drawn regarding the correlation between atomic number and diffusivity in liquid sodium. A summary of Na diffusivity in multiple metallic systems is shown in Table 2. The self-diffusivity of pure Na at 723K is consistent with the values from previous calculations and experiments, considering the errors generated during simulation.

3. Experimental Measurement of Solubility of Lanthanides in Sodium and Cesium

In the experimental work we focused on the solubility of cerium, praseodymium, and neodymium within liquid sodium and liquid cesium. The time dependence to reach the equilibrium concentration was studied in both liquid sodium and liquid cesium. Additionally the temperature dependence of the lanthanides in liquid sodium was investigated.

The method used to measure the solubility was an “inversion crucible” method [5]. For this procedure a tubular crucible of stainless steel was used. One end of the crucible was closed with a cap. At this end of the crucible a solid piece of lanthanide metal and a solid piece of alkali metal was placed in the cap. A mesh, of the same material as the crucible, was placed in the center of the crucible and then the open end of the crucible was closed with a cap. This crucible was placed within a furnace so the cap with the alkali solid and lanthanide solid was at the bottom. The furnace was heated to melt the alkali metal and maintain the entire crucible at the temperature of interest. The crucible was held at a constant temperature for a specific time, and then crucible was inverted 180˚ so the crucible cap previously at the bottom of the furnace was at the top of the furnace. This inversion caused the liquid alkali metal to flow from one end of the crucible through the mesh to the other end of the crucible while the lanthanide solid was filtered from the liquid by the mesh. The crucible was then allowed to

cool. The crucible then contained at one end a solid alkali sample containing a lanthanide concentration of the solubility of the temperature of interest. This solid alkali sample was then dissolved in isopropanol alcohol and the lanthanide concentration was measured via Inductively Coupled Plasma Mass Spectroscopy (ICP-MS).

A sample of the as-received solid alkali metal from the manufacturer was dissolved in isopropanol alcohol and the lanthanide concentration was determined by ICP-MS. This measured concentration was the initial lanthanide impurity concentration in the solid alkali metal. The initial impurity content is listed in Table 3.

TABLE 3: IMPURITY LANTHANIDE CONCENTRATION IN SOLID ALKALI METAL USED IN EXPERIMENTS.

Element	**Sodium (at.%)**	**Cesium (at.%)**
Cerium	2×10^{-7}	2×10^{-7}
Praseodymium	0.6×10^{-7}	2×10^{-7}
Neodymium	2×10^{-7}	4×10^{-7}

Solubility experiments were performed with different equilibration time (30 minutes to 70 hours) to determine the solubility rate. In FIG. 3 the time dependence of the neodymium concentration in liquid sodium at 450 ˚C is shown. The concentration of neodymium reaches an approximately constant concentration in the liquid sodium prior to 30 minutes, as the data suggests a constant concentration from 30 minutes to 72 hours. Over these time dependence tests, the average neodymium concentration was 3.8×10^{-6} at.%.

FIG. 4 shows the time dependence of the concentration of neodymium in liquid cesium at 200 ˚C. The concentration of neodymium in liquid cesium appears to reach a steady concentration prior to 30 minutes, similarly to the liquid sodium time dependence. The average concentration of neodymium for 200 ˚C for during these time dependence tests was 1.7×10^{-5} at.%.

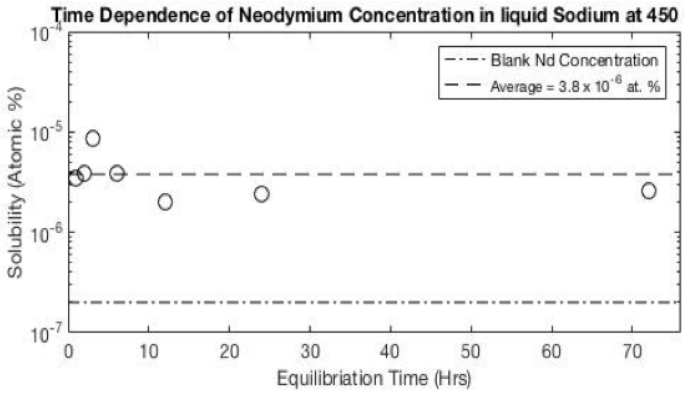

FIG. 3. Time dependence of neodymium concentration in liquid sodium at 450° C.

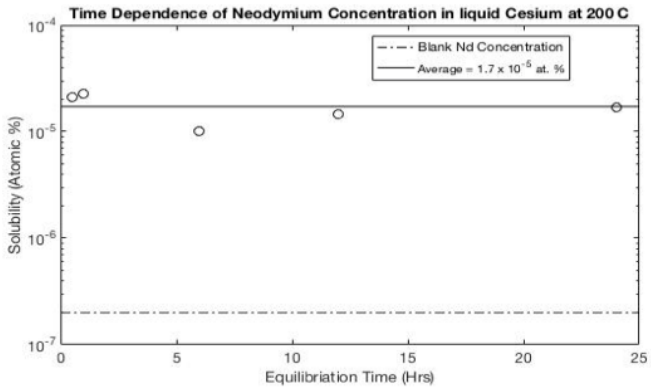

FIG. 4. Time dependence of neodymium concentration in liquid cesium at 200° C.

With the time dependence testing showing the solubility concentration being reached within 30 minutes, temperature dependent tests were conducted with equilibration of 24 hours to ensure equilibrium was reached. In FIG. 5 the results of the temperature dependence of the lanthanides in liquid sodium are shown. Over the temperature range of 450 to 550 ˚C, the lanthanides show an increase in solubility with temperature. Extrapolation of data with an Arrhenius equation to 1000 K gives a solubility of 10^{-3} at.%, which is low compared with the previous calculation (0.8 at.% [2]). A further investigation will be done to find out the potential reasons for the disagreement.

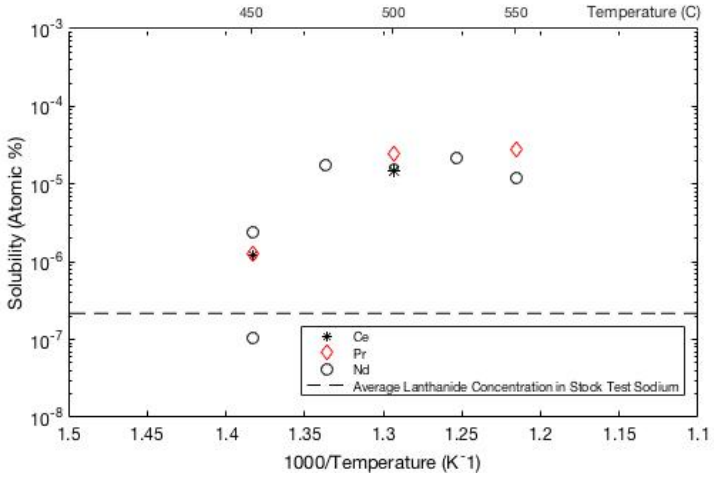

FIG. 5. Temperature dependence of lanthanides in liquid sodium.

4. Modeling of Lanthanide Transport in a Single Liquid Metal Filled Pore with a 1D Temperature Profile

A model was constructed in order to study the feasibility of the proposed “liquid-like transport” of lanthanides in liquid filled pores, and is briefly portrayed in FIG 6. Ln that is generated in the fuel will diffuse due to concentration and temperature gradients. At the pore interface, a first-order kinetic reaction is used to approximate the transport of Ln across the boundary through the utilization of a driving force based on Ln chemical potential approximated by how far the Ln is above or below solubility in the material. Similar to Ln in the fuel, Ln in the pore will transport based on both concentration and thermal gradients. Additionally precipitation will occur if the local concentration is greater than the solubility limit.

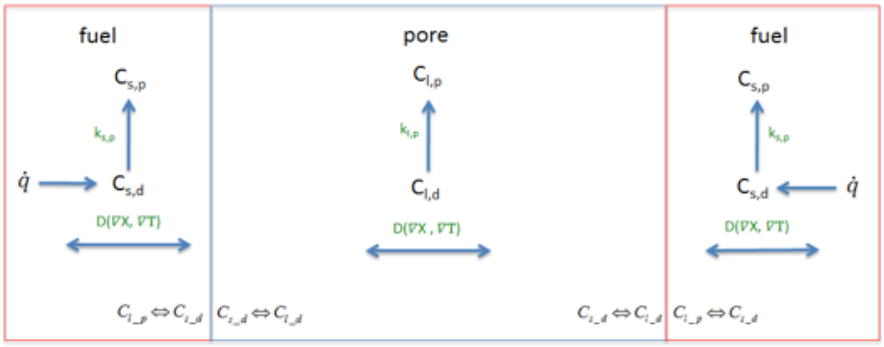

Applied kernels in BISON

$$\frac{\partial C_{s,p}}{\partial t} = Q_{s,p}$$

$$\frac{\partial C_{s,d}}{\partial t} = Q_{diffusion} - Q_{s,p} + \dot{q}$$

$$\frac{\partial C_{l,p}}{\partial t} = Q_{l,p}$$

$$\frac{\partial C_{l,d}}{\partial t} = Q_{diffusion} - Q_{l,p}$$

Precipitation kinetics in the fuel

$$Q_{s,p} = \begin{cases} 4\pi R C_{sink} D_{s,d} \cdot \frac{(C_{s,d} - C^0_{s,d})}{C^0_{s,d}} \cdot \left(1 - \frac{C_{s,p}}{C_{Ln\_pure}}\right) \cdot C_{s,d} & (C_{s,d} > C^0_{s,d}) \\ 0 & (C_{s,d} \le C^0_{s,d}) \end{cases}$$

Precipitation kinetics in the pore

$$Q_{l,p} = \begin{cases} k_{l0} \cdot D_{l,d} \cdot \frac{(C_{l,d} - C^0_{l,d})}{C^0_{l,d}} \cdot (1 - \frac{C_{l,p}}{C_{Ln\_pure}}) \cdot C_{l,d} & (C_{l,d} > C^0_{l,d}) \\ 0 & (C_{l,d} \le C^0_{l,d}) \end{cases}$$

Diffusion kinetics

$$Q_{diffusion} = -\nabla \cdot \vec{J}$$

$$\vec{J} = -D\left(\frac{\partial C}{\partial x} + \frac{Q^* C}{RT^2}\frac{\partial T}{\partial x}\right)$$

FIG. 6. Schematics of Ln diffusion and reactions.

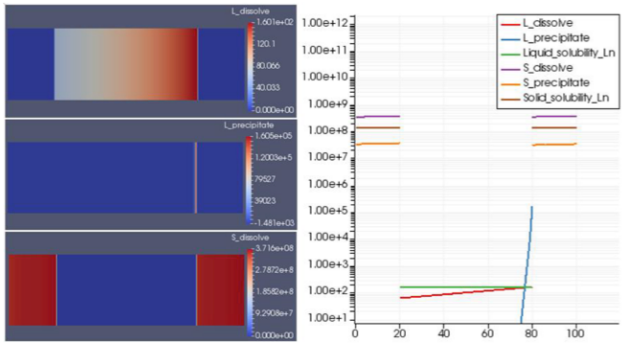

FIG. 7. Distribution of Ln concentration along 100 μm, at 10 at.% burnup. The temperature is decreasing with a gradient of 5×10^{-2} K/μm from 855 K on the left to 850 K on the right. An isolated pore is introduced between two fuel blocks.

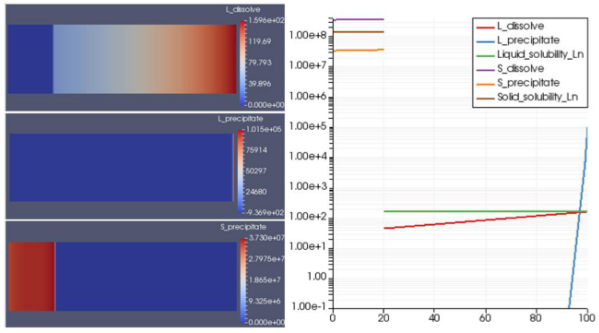

FIG. 8. Distribution of Ln concentration along 100 μm, at 10 at.% burnup. The temperature is decreasing with a gradient of 5×10^{-2} K/μm from 855 K on the left to 850 K on the right. There are two blocks: U-Zr fuel on the left and a Na-filled pore on the right

As shown in FIG. 6 four different Ln concentrations are defined as variables and restricted in corresponding blocks: $C_{s,p}$ and $C_{s,d}$ exist in the fuel; $C_{l,p}$ and $C_{l,d}$ are in the pore. At the beginning of irradiation, Ln is generated as $C_{s,d}$ in the fuel. $C_{s,d}$ will precipitate out as $C_{s,p}$ once the solubility limit is exceeded. Analogously the liquid-state precipitation occurs in the pore. The reaction between Ln solutes $C_{s,d}$ and $C_{l,d}$ occurs at the fuel-pore interface and is approximated by first-order kinetics model. As related to Ln chemical potential, Ln solubility in different media is used to determine the Ln flux across the interface. After precipitation occurs in the pore, the reaction between Ln solutes $C_{s,d}$ and $C_{l,p}$ will start. The liquid-state diffusivity D_l is used for $C_{l,d}$ in the pore, while the solid-state diffusivity D_s applies to $C_{s,d}$ diffusion in the fuel. Soret effects, which drive the diffusion alonge the temperature gradient, are included for the diffusion process with the respective heat of transport Q^*. Details of this model will be discussed in further depth in a future publication. We implemented this pore model into BISON and used typical conditions from an X447 subassembly, EBR-II U-10Zr fuel rod [see Ref. 7]. The previously discussed solubility limits and diffusion coefficients were used in simulations.

In FIGs. 7 and 8 we apply the conceptual model to a single idealized sodium filled pore configuration (FIG. 7) as well as a idealized sodium filled interconnected pore network (FIG. 8). Using the parameter settings shown in Table 4, we observed that at 10 at.% burnup the dissolved lanthanide in the fuel will be oversaturated in the fuel, in small sodium filled isolated pores, and in sodium filled long interconnected pores (see purple "$S_{dissolve}$" on the left side of both figures). The precipitation kinetics in both the fuel and the pore considers a driving force due to the difference between oversaturated dissolved lanthanide concentration and solubility limit.

As long as oversaturated conditions occur, then precipitation in isolated or interconnected porosity are possible outcomes. The dissolved lanthanides diffuse to the cold side of the pore, exceeding the solubility limit in the liquid, resulting in precipitation on the cold side of the pore. Originally it was thought that lanthanides that had precipitated on the cold side of isolated pores could also diffuse back into the solid fuel with an enhanced diffusion mechanism so that isolated pores could act like pumps causing accelerated diffusion through a fuel-pore-fuel configuration. However, the mechanism at the fuel-pore interface based on the Ln chemical potential causes isolated pores to act like a lanthanide sink as opposed to a pump. In the case of sodium filled interconnected pores, lanthanides are able to diffuse to inner clad surfaces and precipitate in the vicinity. Initial results show that lanthanide transport from fuel to the cladding can be dramatically accelerated only when the pores are interconnected or there are sodium filled cracks present. A fair question remaining to be investigated surrounds the number of unknown rate constants used, which are listed in Table 4. We perturbed the parameters R, C_{sink}, $k_{l,0}$, $k^{l,d}$, $k^{l,p}$, Q^*_{solid}, Q^*_{liquid}, by up to two orders of magnitude and performed various runs in search of results opposite of our current conclusions. Yet so far our results still suggest that isolated pores will act as lanthanide sink and the transport mechanism of lanthanides from fuel to the cladding has to occur through interconnected pores and cracks filled by sodium.

TABLE 4: PARAMETER SETTINGS USED FOR BISON SIMULATIONS.

Kinetics	**Parameter**	**Value**
Precipitation	$R \times C_{sink}$ (μm^{-2})	0.01
	$k_{l,0}$ (μm^{-2})	0.001
	Solid solubility (at. frac)	0.003
	Liquid solubility (at. frac)	$(1.39\times10^{-7}) \times \exp(-0.213/[T\times k_B])$
Interface Reaction	$k^{l,d}$ (μm^{-4})	10^3
	$k^{l,p}$ (μm^{-4})	10^4
Diffusion	Solid D (cm^2/s)	$(6.31\times10^{-8}) \times \exp(-1.71/[T\times k_B])$
	Liquid D (cm^2/s)	$(6.66\times10^{-4}) \times \exp(-0.223/[T\times k_B])$
	Solid Soret Q^* (eV)	10
	Liquid Soret Q^* (eV)	20
Source	$\dot{q}$ ($atom\times s^{-1}\times\mu m^{-3}$)	7.94

5. Conclusions

The solubility of lanthanides is experimentally measured and calculated using AIMD simulations. The experimental results indicated that the solubility of cerium, praseodymium, and neodymium in liquid sodium varied from 2×10^{-5} to 5×10^{-5} at.% between 450 to 550 °C. which are lower than results obtained from AIMD simulations. The time dependence of the solubility is also obtained from experiments conducted at different equilibration times. Our results showed that the solubility limit is reached within 30 minutes, indicating that the dissolution rate is fast relative to diffusion, thus suggesting that lanthanide transport would be diffusion limited. Additionally the diffusivity of lanthanides in sodium and cesium is calculated by simulation. A conceptual pore model was developed to better describe the Ln transport behavior through the fuel. Our results suggest that isolated pores will act as a lanthanide sink. However, isolated pores can be expected to become part of the interconnected pore network with increasing burnup, and the transport mechanism of lanthanides from fuel to the cladding occurs generally through interconnected pores and cracks filled by sodium.

6. Acknowledgments

We acknowledge support from the U.S. Department of Energy, Office of Nuclear Energy through the Nuclear Energy University Program (Project 14-6482). Advanced Fuels Campaign of Fuel Cycle Research and Development Program also supported the pore modeling with BISON.

7. References

[1] MARIANI, R.D., et al., “Lanthanides in metallic nuclear fuels: Their behavior and methods for their control”, J. Nucl. Mater. **419** (2011) 263–271.

[2] SAMIN, A., et al., “Ab initio molecular dynamics study of the properties of cerium in liquid sodium at 1000 K temperature”, J. Appl. Phys. **118** (2015) 234902.

[3] XIANG, L., et al., “Ab-initio molecular dynamics study of lanthanides in liquid sodium”, J. Nucl. Mater. **484** (2017) 98-102.

[4] SWISHER, J.H., Solubility of Iron, Nickel, and Cobalt in Liquid Potassium and Effect of Oxygen Gettering Agents on Iron Solubility, NASA-TN-D-2734, NASA Lewis Research Center, Cleveland, OH, (1965).

[5] BELASHCHENKO, D.K., “Application of the embedded atom model to liquid metals: liquid sodium”, High Temp. **47** (2009) 494-507.

[6] MEYER, R.E., NACHTRIEB, N.H., “Self‐Diffusion of Liquid Sodium”, J. Chem. Phys. **23** (1955) 1851-1854.

[7] PAHL, R.G., PORTER, D.L., CRAWFORD, D.C. WALTER, L.C., “Irradiation behavior of metallic fast reactor fuels,” Journal of Nuclear Materials, Volume 188, June 1992, Pages 3-9